Microelectronic Engineering 107 (2013) 210–218

Contents lists available at SciVerse ScienceDirect

Microelectronic Engineering

journal homepage: www.elsevier.com/locate/mee

Synthesis of carbon nanotubes and graphene for VLSI interconnects

J. Robertson *, G. Zhong, S. Esconjauregui, C. Zhang, S. Hofmann

Engineering Department, Cambridge University, Cambridge CB2 1PZ, United Kingdom

ARTICLE INFO

Article history:
Available online 29 August 2012

Keywords:
Interconnects
Carbon nanotubes
Graphene
Chemical vapour deposition

ABSTRACT

The synthesis of carbon nanotubes and multi-layer graphene for use as VLSI interconnects is reviewed. It is shown that a variety of catalyst pre-treatments can be used to grow vertically aligned carbon nanotube forests with a very high density by chemical vapour deposition, obtaining area densities of order 1.4×10^{13} cm^{-2}. For carbon-based horizontal interconnects, there are three available processes; the direct horizontal growth of carbon nanotubes, the flipping down of vertically oriented carbon nanotubes, or the catalytic growth of multilayer graphene. Graphene CVD should adopt lower temperature catalysts such as Ni or Co alloys for this application. It is emphasised that the growth methods must be compatible with integration.

1. Introduction

The continued scaling of device dimensions in integrated circuits has led to the replacement of many of the traditional materials, such as the use of strained silicon for the channels or the use of high dielectric constant oxides such as HfO_2 to replace SiO_2 as the gate dielectric in the field effect transistors. In the same way, continued scaling will lead to the current density carried in interconnects exceeding the electro-migration limit of copper [1], as shown in Fig. 1. Only carbon in the form of graphene or carbon nanotubes (CNTs) can carry higher current densities of order 10^8 A/cm^2, due to their strong covalent bonding and lack of electromigration [2–4]. However, carbon nanotubes or graphene presently do not have sufficient performance to replace copper, and there are also severe integration issues to be overcome with both materials. This paper describes how the growth of CNTs and graphene needs to be controlled in order to satisfy these requirements [5–21]. There have been several reviews of the use of CNTs and graphene for interconnects [14,21]. The main groups working on CNT interconnect fabrication have been the Infineon group [7], the Fujitsu/Mirai group [14] and recently the Viacarbon group [18]. In addition, there have been numerous analyses of the performance of CNTs as interconnects [4].

We will first describe work with CNTs. CNTs are potentially useful for interconnects because of their high current carrying capacity, their ability to be grown in high aspect ratio structures, and that they do not need to be surrounded by diffusion barrier liners. The latter points are useful for both standard vertical interconnects and the through wafer vias. Note that the CNTs must be grown in place by, for example, chemical vapour deposition (CVD). They cannot be grown elsewhere and then placed in the vias, as this is not a scalable manufacturable process.

The problem for carbon nanotubes is that they are one-dimensional conductors, so that they introduce a quantum of conductance as a series resistance [17]. Hence it is necessary to parallel many CNTs together in order to reduce the total resistance of the interconnect to below that of the copper equivalent, see Fig. 2. This requires us to develop CNT densities or CNT wall densities to of order 3×10^{13} cm^{-2}, which is extremely high by present standards. This amounts to a spacing Fig. 2 emphasises that the gain from using CNTs is greater for the longer horizontal interconnects than it is for the shorter vertical interconnects or vias [16]. On the other hand, growing for vias is the easier problem. Fig. 3 shows the difficulty of achieving the needed area density, by comparing it to the area density of CNT forests grown by recent workers [21–31].

Thus the requirements for using CNTs as vertical interconnects are, (1) a large nanotube area density, (2) a process integration scheme to ensure conducting bottom and top contacts, (3) processes carried out at 400C or lower, for CMOS compatibility.

2. Vertical interconnects

CNTs are presently grown by CVD using a transition metal as a catalyst. The most effective catalysts for CNT growth are Fe, Co and Ni. In the CVD process, the catalyst must first be converted in a pre-treatment step into its active form, which is as a series of nanoparticles. Growth is then carried out from a hydrocarbon source gas such as ethylene or acetylene [22,32], usually diluted with hydrogen. The hydrocarbon molecules will dissociatively absorb on the catalyst surface, releasing carbon atoms, which then diffuse through or over the catalyst surface to re-assemble as the carbon nanotube. Generally, the most dense CNT forests grow with the catalyst at the root (root growth) rather than at the tip. Also, one

* Corresponding author. Tel.: +44 1223 748331; fax: +44 1223 332662.
E-mail addresses: jr@eng.cam.ac.uk, jr214@hermes.cam.ac.uk (J. Robertson).

0167-9317/$ - see front matter © 2012 Elsevier B.V. All rights reserved.
http://dx.doi.org/10.1016/j.mee.2012.08.010

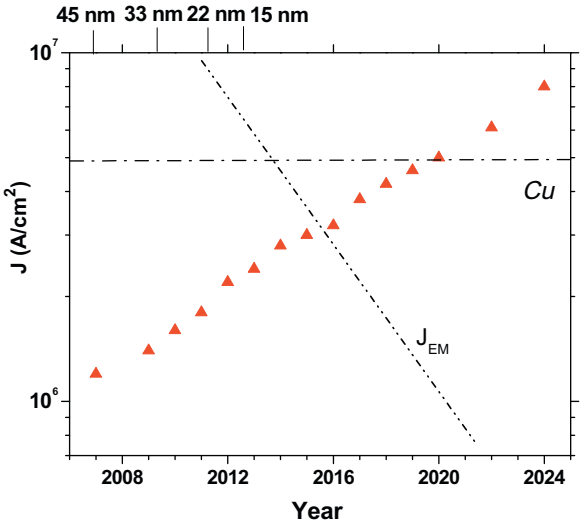

Fig. 1. ITRS Roadmap of current density carried by interconnects vs year.

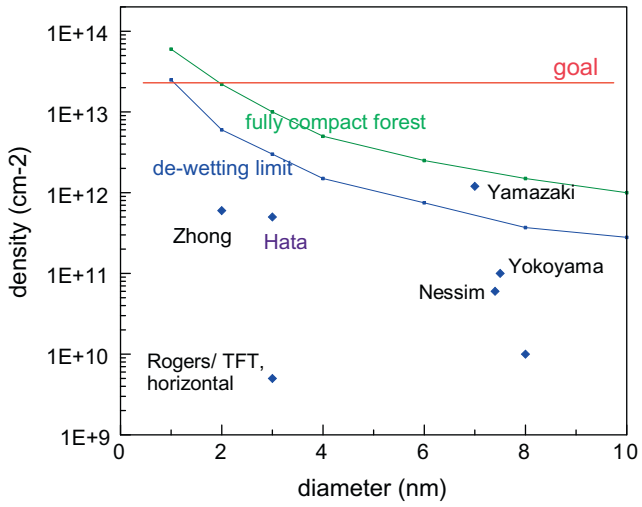

Fig. 3. Variation of area density with nanotube diameter, for some high density, vertically aligned nanotube forests grown by various groups.

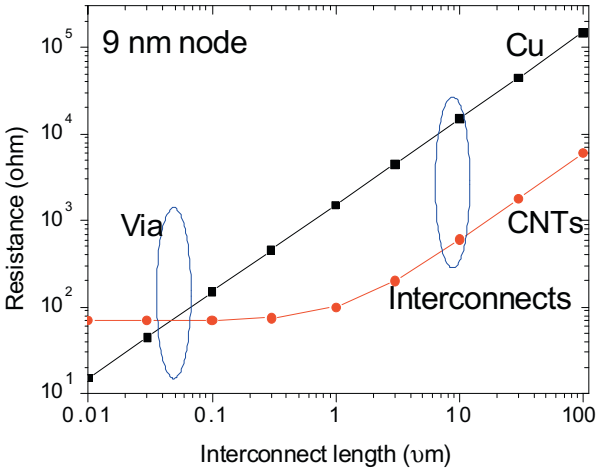

Fig. 2. Comparison of interconnect resistance vs interconnect length for copper interconnects and SWNT interconnects for a nanotube density of 10^{13} cm^{-2}.

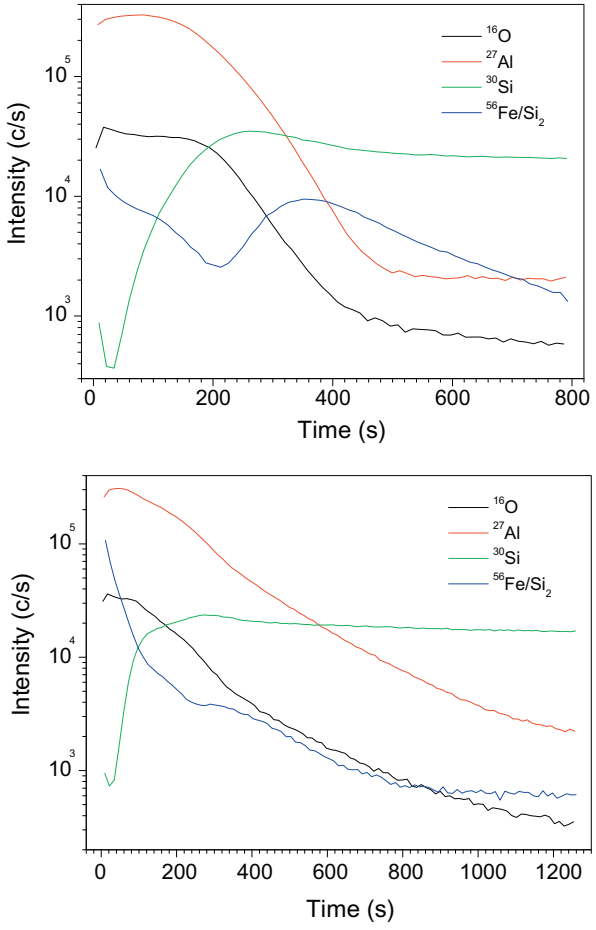

Fig. 4. SIMS depth profile into a layer of 0.4 nm Fe on 5 nm Al_2O_3 on Si wafer, for case of (a) normal Al_2O_3, and (b) plasma oxidation densified Al_2O_3.

nanotube grows from each catalyst nanoparticle. Thus, the problem of maximising nanotube density is to maximise the area density of the catalyst nanoparticles.

The catalyst nanoparticles could be created by nanoparticle deposition from a cluster beam source [33], or by electrodeposition, but the lowest cost and most effective method uses a surface energy effect of the catalyst on its support layer – the layer underneath [34].

We use the minimisation of total surface energy to convert the as-deposited catalyst film into a series the active nanoparticles. The process generally involves a special pre-treatment step, while heating up to the growth step, sometimes in a specially controlled reducing atmosphere or plasma process before the growth gas is admitted, to control the catalyst area and anchor the catalyst to the layer beneath. The catalyst will convert into nanoparticles because this lowers its surface energy, if it is on a low surface energy oxide. However, the problem is that the oxide is often an insulator.

The most effective catalyst – support combination for CNT forests is presently an Fe catalyst on Al_2O_3 support [35]. The preferred conducting support layers are TiN, $CoSi_2$ or Ta, which are also diffusion barriers [10].

We now consider ways to maximum the area density of CNTs. Fig. 3 shows the density of existing 'high density' vertically aligned CNT forests in the literature [23,25,26,28,12,13]. The density is not high, as the nanotubes in a typical forest only cover about 5% of the available area, with a diameter of ~3.0 nm and a density of 5×10^{11} cm^{-2}. The data in Fig. 3 shows that there are two ways

to increase the density; increase the packing fraction, or decrease the mean CNT diameter.

When the thin film catalyst is converted into nanoparticles, the diameter D of the nanoparticles is proportional to the thickness of the initial film, h. Thus, the nanoparticle density N varies with h as

$$N \sim 1/h^2 \quad (1)$$

We have studied three ways of increasing N.

The simplest way to increase N is to decrease the nanotube diameter by decreasing h. Growth of typical forests already uses catalyst films that are very thin, h ~ 1 nm. This means that a consider amount of the catalyst can diffuse inside the support layer during heating and be unavailable for growth. Now, Al_2O_3 was chosen because it has a low surface diffusion [35], but it can be porous, so inward diffusion is not well controlled. Thus, it can be difficult to decrease h further because this affects yield. One way to achieve this is to use plasma oxidation to densify the Al_2O_3 film (or other film) below the catalyst and so inhibit subsurface diffusion [36]. The effect of this is seen in Fig. 4 in SIMS data on the inward diffusion of Fe. Fig. 4a shows that there is a peak in the Fe diffusion profile where it hits the Si substrate, evidence for inward Fe diffusion, but this peak is missing for the case of densified Al_2O_3 in Fig. 4(b). This allows the use of Fe layers of thickness down to 0.3 nm. In addition, to ensure the maximum nucleation from the catalyst nanoparticles, the partial pressure of the growth gas acetylene has been increased.

Fig. 5(e) shows TEM images of the resulting nanotubes. They are single walled nanotubes (SWNTs), and their average diameter is measured to be 1.1 nm. This is much less than the typical 3 nm of standard forests. Fig. 5(a–d) shows SEM images of the sides of the forest. The CNTs are seen to be well-aligned. The density is largely uniform over the forest, but the density can be lower at the forest base, just above the catalyst. This might be because growth has terminated due to poisoning for some of the catalyst particles. It is necessary to ensure that growth stops deliberately, not by catalyst poisoning. Fig. 5(f) shows the diameter distribution evaluated from Fig. 5(e), with an average diameter of 1.1 nm. Fig. 6 shows the radial breathing mode spectra measured by resonant Raman, which confirms the TEM estimate of the diameter distribution.

The area density of the forests can be measured in three ways [36]. The first but least accurate way is by counting in an SEM image. The second way is to use liquid-induced compaction. This uses the surface tension of a liquid such as isopropyl alcohol to compact the forest into locally dense regions. The density in these regions can be measured by TEM, from the inter-tube spacing, or can be estimated by X-ray scattering. Then, the area reduction on the top surface is measured by SEM, see Fig. 7. The original density is then derived from the ratio of these areas. This method is useful for estimating the density within the confined space of a via [18].

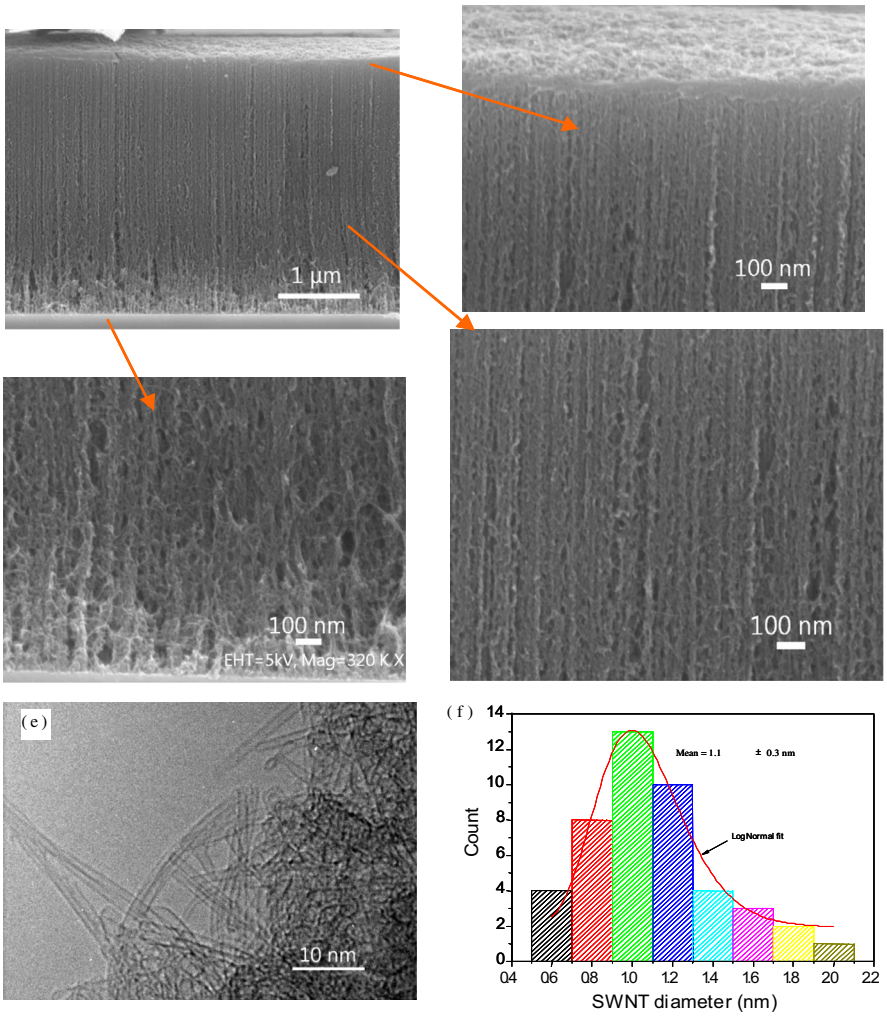

Fig. 5. (a–d) SEM images of the sides of a high-density forest grown on densified Al_2O_3 for 0.4 nm Fe catalyst, at 8% C_2H_2 in H_2, 20 mbar gas pressure, at 680 °C. (e) High resolution TEM images of the nanotubes showing them to be mainly single walled. (f) Derived diameter distribution.

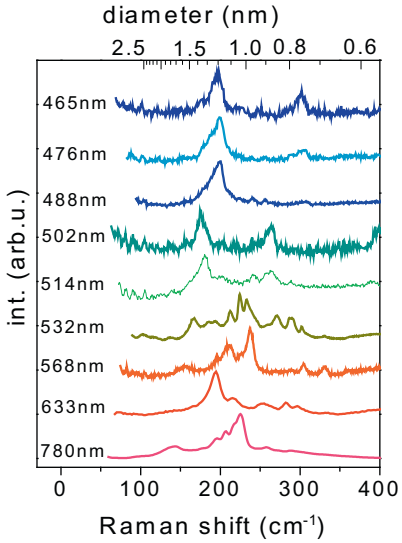

Fig. 6. Resonant Raman spectra of radial breathing modes of the forest shown in Fig. 5, and the diameter distribution from mode assignments, showing that the nanotube diameters are mostly below 1.5 nm.

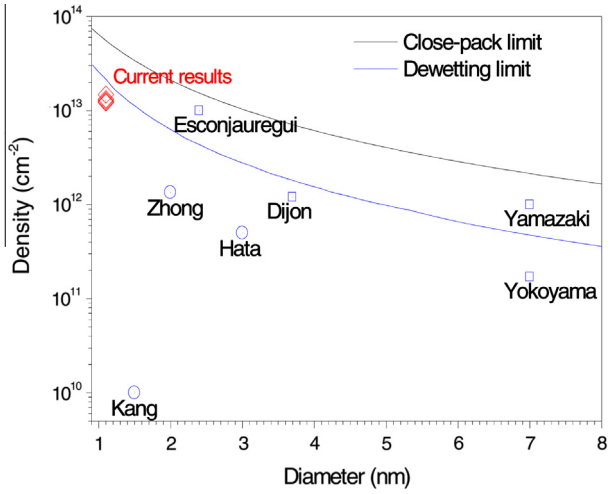

Fig. 8. Measured densities of forests grown on the densified Al_2O_3 support layer, and by the cyclic catalyst deposition process.

The third and most reliable method is by weight gain. This is only possible for blanket films. The weight gain during growth is measured on a microbalance, together with the sample area and the height of the forest. Then the CNT diameter is derived from TEM images, for SWNTs and for each wall for MWNTs. This is used to calculate the weight per unit length of the nanotube. The area density is then calculated from the ratio of weight gain to weight per unit length.

Using the weight gain method, we have been able to achieve an area density of order $1.4 \times 10^{13}\,cm^{-2}$ for the 1.1 nm diameter tubes, see Fig. 8 [36]. Thus, the density has been increased by a factor of 30, Fig. 8.

A second way to increase the area density is to use multiple cycle catalyst deposition [37], as shown schematically in Fig. 9. Eq. (1) says that thicker catalysts give thicker CNTs and lower densities. If we deposit two layers of catalyst, upon heating up to the growth temperature, these would normally sinter together into a single layer, with a larger diameter and a lower density. However, it is sometimes possible to restructure the first layer by annealing, then after cooling back to room temperature, depositing a second catalyst layer and annealing this and avoid it sintering into the previous layer. This requires the first layer to be immobilised, so that it does not merge with the next layer. If this can be done, then the density can be increased linearly with the number of cycles.

Fig. 10 shows a SEM image of the CNTs from this process, showing an average diameter of 2.4 nm, and the SEMs of the forest. The

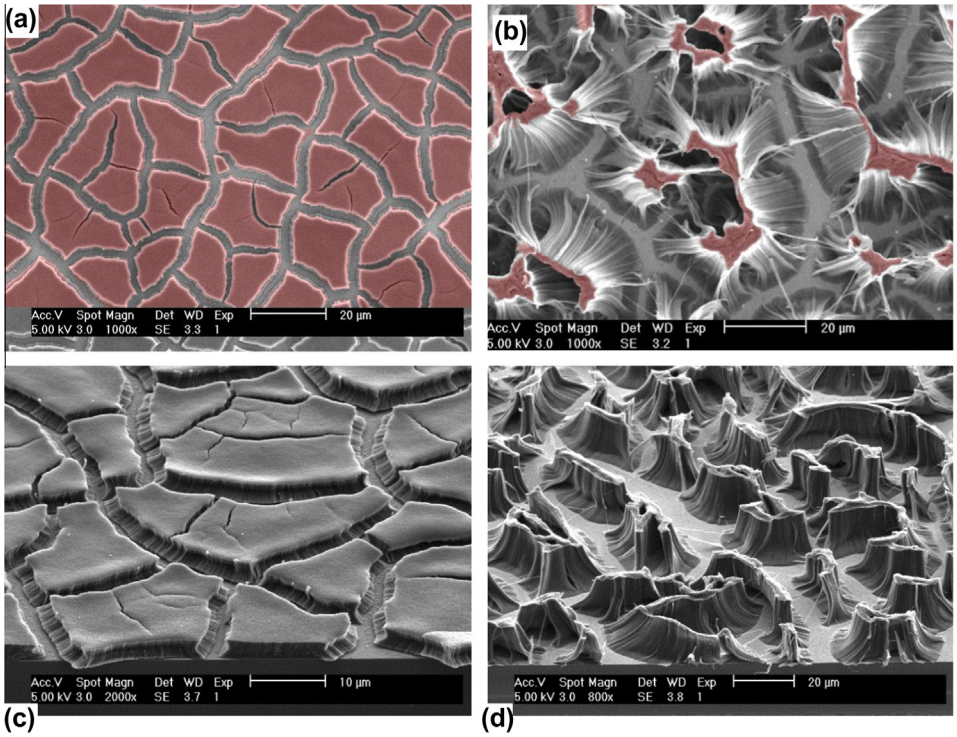

Fig. 7. Showing the effects of liquid induced compaction on a normal vertically aligned forest (right) and a high density forest grown on densified Al_2O_3 support layers (left). Vertically and side views.

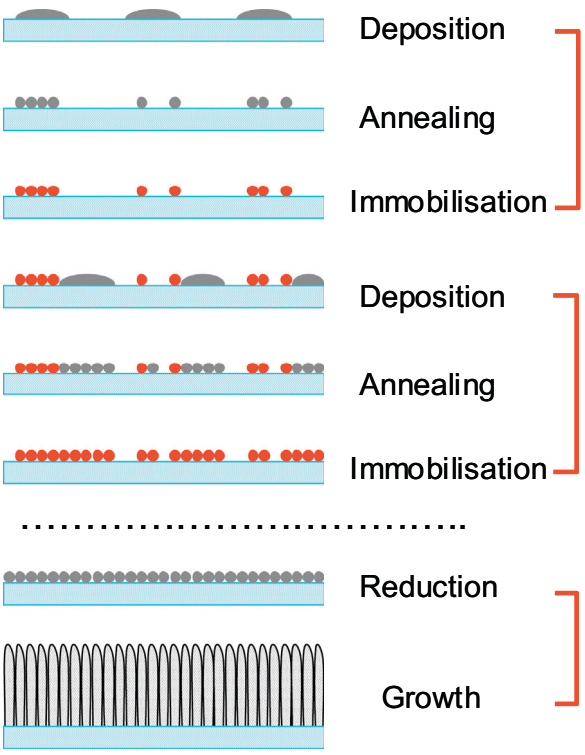

Fig. 9. Schematic of the cyclic catalyst deposition process [37].

CNTs are mainly double walled. The weight gain method has found that an area density of about 1.3×10^{13} cm^{-2} can be achieved by this method. This is also a very high number, and an increase of order 25 over previous densities.

The third method for increasing density was developed by Yamazaki et al. [13]. It involves a 3 step process, as shown schematically in Fig. 11. The first step uses an Ar plasma to restructure the catalyst into nanoparticles. The second step uses a short low temperature hydrocarbon plasma to deposit a thin layer of carbon

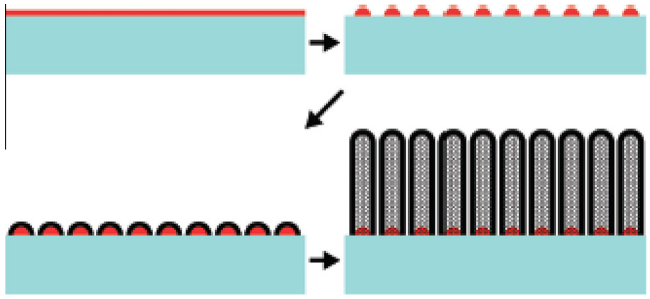

Fig. 11. Schematic of the 3 step catalyst pre-treatment method used by Yamazaki to increase nucleation density.

to immobilise the catalyst nanoparticles. Then the growth proceeds as normally. The original work [13] claimed a density of 10^{12} cm^{-2}, as determined by counting, for multiwalled nanotubes of diameter of about 7 nm. We have repeated this process, and achieved a smaller diameter of 4 nm and a density of over 10^{12} cm^{-2} as determined by weight gain [38]. The results are summarised in Fig. 8.

These growth results must be incorporated into a full process flow, as shown schematically Fig. 12. Catalyst is first deposited by ion beam sputtering at the bottom on the via holes. Growth occurs. Then, the via holes are back filled by a filler such as atomic layer deposited Al_2O_3 or spin-on glass or similar, to hold the CNTs in place. The wafer is then planarised by chemical mechanical polishing (CMP). This cuts the CNTs and exposes their wall ends. Then the top electrodes are deposited. The top contacting process must avoid oxidation of the bottom contacts or other introduction of any resistive layer. Details of this can be found in Dijon et al. [18].

Dijon [17,18] was able to transfer the high density growth recipes to work within small diameter via holes. The area densities are now confirmed by the liquid induced compaction method.

Plasma pre-treatment of the catalyst can be used to enforce the root growth mode, which seems to be a requirement for obtaining the high-density vertically-aligned forests [39–42]. Extensive in situ XPS and XRD have been used to track the chemical state

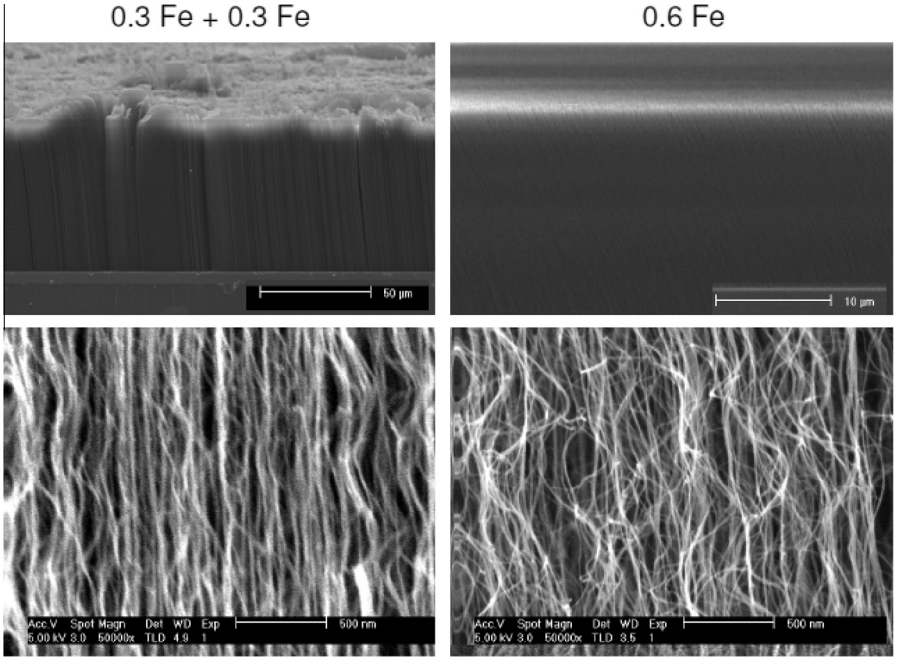

Fig. 10. Transverse SEM images of CNTs grown by 2 layer catalyst, and single layer catalyst.

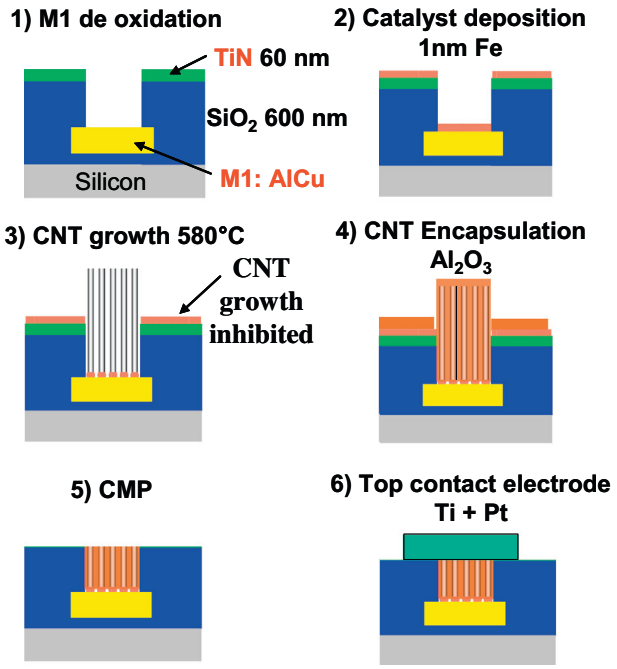

Fig. 12. Schematic of the process flow for grown and integration of vertical CNT interconnects, from Dijon et al. [18]. A similar process is used by Awano et al. [14].

of the catalyst and support layers during growth conditions [43,44]. This checks where support metals are present as metals or oxides, and whether it is amorphous or crystalline. For example, it is found essential to keep growth on Ta below 550C otherwise a polycrystalline oxide develops that allows catalyst to diffuse rapidly away from the surface by grain boundary diffusion [44]. Self aligned patterning of the growth catalyst can be achieved using CoSi2, for example at the base of vias [45].

3. Horizontal interconnects

There are four possible ways to use carbon materials for horizontal interconnects, either grow CNTs horizontally, grow them vertically and then flip them down to be horizontal, use plasma or pyrolytic carbon, and finally graphene.

It is possible to grow CNTs horizontally, if the catalyst can be patterned on a vertical side-wall surfaces. This requires specially constructed substrates. To date, the area densities achieved by this method [46–48] have been typically 10 times lower than those achieved for vertical growth. The alignment of CNTs in forests arises because the high packing density forces them to grow aligned, and in a vertical direction. The problem for horizontal growth is that the CNTs need to be confined into a space so that a similar effect forces them all to grow in the same direction, and many structures do not do this. A second factor behind the lower area density for horizontal growth is simply that there has been much less effort on this subject. There needs to be more work on thinner catalyst layers.

The second method for horizontally aligned CNTs is to grow patterned arrays vertically and then use liquid wetting and surface tension effects to flip them over to a horizontal direction, as first shown by Hayamizu et al. [49]. This method uses the existing methods to grow high-density, vertically-aligned forest arrays. A problem with flipping is that the direction of flipping needs to be accurately controlled to hit the receiving electrode. One possibility is to use a landing zone defined by a different surface energy to give a preferred landing position. Fig. 13 shows a case of vertical CNT arrays flipped into the horizontal direction.

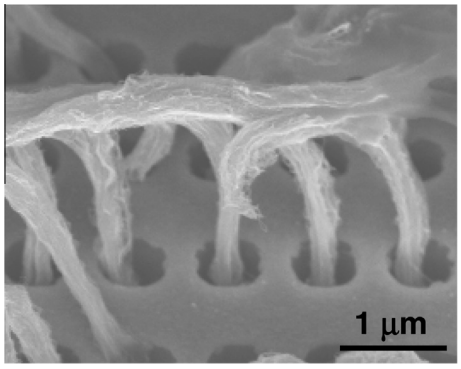

Fig. 13. SEM image of vertically grown CNTs, flipped down for horizontal alignment by the liquid contact method. Acknowledgement J. Dijon et al.

In the third method, Graham et al. [50] have developed pyrolytic carbon as a conducting layer made from carbon, for use in various microelectronic systems. This method can involve CVD or PECVD but no catalyst. It is easy to make, and can be easily patterned. This is a possibility for interconnects, but the problem is do they have sufficiently high conductivity.

4. Graphene

Graphene or more accurately multi-layer graphene could be a very useful material for horizontal interconnects because of its potential for high conductivity and high current carrying capacity. The question is how to make it and how to make the process compatible with standard process flow.

There are five ways to make graphene-like material; the exfoliation of graphene by Scotch tape, the graphene oxide route, the sublimation of Si from SiC faces at 1300 °C, catalytic CVD onto metals, and the catalytic solid-state transformation route. The first three methods are not relevant to interconnect applications due to either using a non-scalable transfer method, or using too high a temperature.

The catalytic CVD is relevant, but it presently involves the growth onto metals (Ni or Cu) at around 950–1000 °C and then an adhesive transfer on a polymer to the receiving surface [51–56]. The transfer process is also *not relevant* to interconnects - the graphene must be grown directly in place. On the other hand, the graphene CVD literature has a strong focus on growing monolayer or few layer graphene, whereas for interconnect applications 5–10 layers or more are suitable.

Graphene CVD has in fact been studied for many years in the surface science community, without them fully realising. Few layers have been grown on various catalyst metals such as Ru, Pt, Pd. More recently, one of the first direct growths was on Ni by Reina et al. [51]. The field became active when it was pointed out by Ruoff [52] that CVD on copper could be self-limiting to a single layer.

Xi et al. [53] have shown that the CVD on Cu and Ni are different processes, Fig. 14. They used the Raman mapping of graphene layers after sequential gas exposures to ^{12}C and ^{13}C isotopically enriched hydrocarbons. Growth on Ni (or Co etc.) involves the dissociation of the hydrocarbon on the metal surface and the dissolution of carbon into the metal, and its subsequent precipitation onto the metal surface after cooling, or after the metal surface layer becomes super-saturated with carbon and the carbon arrival rate exceeds the rate at which it can diffuse away into the metal bulk at that temperature [55,56]. On the other hand, for Cu, the hydrocarbon dissociates on the copper surface and because of the very low solubility of C in Cu, even at the melting point, the graphene layers grow by the surface diffusion of C over the exposed Cu to

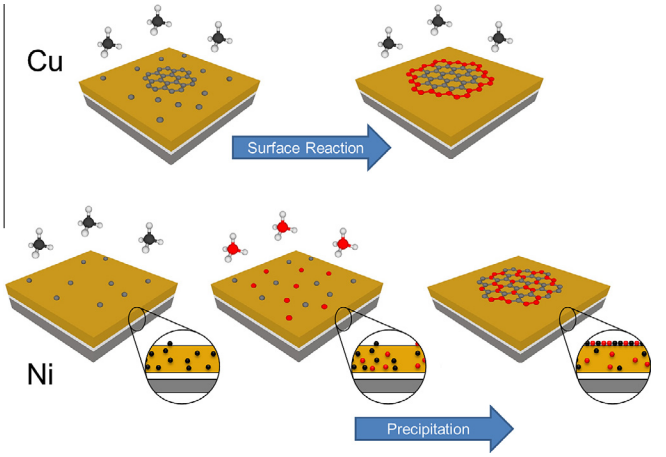

Fig. 14. Schematic comparison of the graphene growth mechanism on Cu and on Ni.

find an edge of a graphene grain. The C atoms add at the edges of existing graphene grains, making them grow outwards. Carbon does not stick or dissociate on the graphene itself. Once the Cu is covered, in theory growth stops, because there is no longer an Cu catalyst exposed. This self-limiting growth should in theory lead to monolayer growth.

The advantage of Cu is that it is a very inefficient catalyst, as can be seen from the volcano plot of catalyst efficiency against element (Fig. 15) [57]. Thus the self-limiting growth leads to monolayer graphene, which is desired for many applications. However, this factor is not particularly important for interconnects. The disadvantage of CVD on Cu is that it requires pre-annealing and growth at quite high temperatures. The annealing in hydrogen is to remove surface oxide which causes surface steps. The problem is that at 950–1000 °C the evaporation rate of Cu is so high and it pollutes the vacuum system [55].

Ni (or Co) is a preferable growth catalyst for graphene used for interconnects. Ni is a more efficient catalyst than Cu, so a lower temperature can be used. Also, the formation of multiple graphene layers is not a problem. The number of layers formed can be controlled by controlling the total carbon exposure (pressure times time), as noted by Weatherup et al. [55] and Kondo et al. [58,59]. A low temperature of order 450–560 °C is useful so that the C does not diffuse into the underlying metal [58].

Good quality graphene layers can be achieved by limiting the nucleation density – the opposite of our desire in CNT growth. This

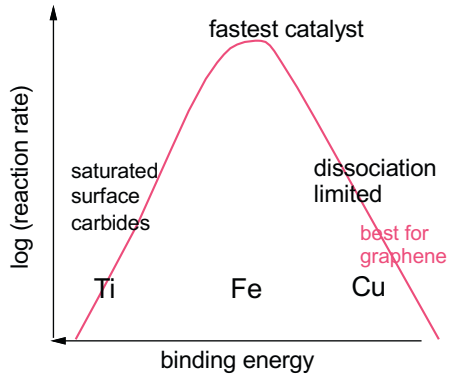

Fig. 15. Volcano plot of catalyst efficiency for carbon nanotube growth, indicating how an inefficient nanotube catalyst is good for CVD of graphene, as it will lead to fewer layers.

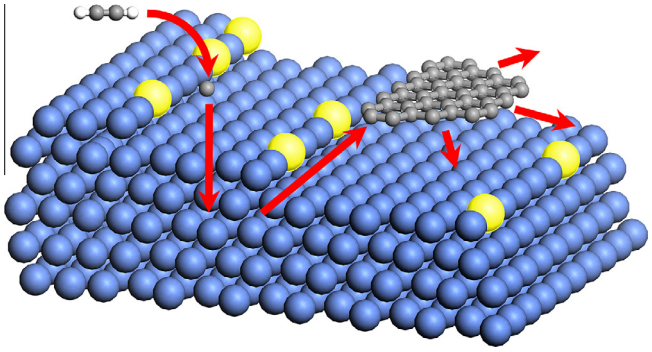

Fig. 16. Schematic of how Au atom decoration of steps reduces graphene nucleation, thus leading to larger grain sizes and better coverage.

was achieved by Weatherup et al. [55] by using Au–Ni alloys. Here, the Au atoms decorate and poison the surface step sites of the Ni terraces, which are the normal nucleation points of C growth on Ni surfaces (Fig. 16). This leads to much larger graphene grain sizes on Ni. A second factor is to use a microwave plasma to pre-dissociate the hydrocarbon precursor, if methane is used [60,61]. Microwave plasma-assisted CVD is found to easily give growth of good quality graphene with a good Raman signature at 450 °C [60]. This is compatible with CMOS requirements. Microwave or remote RF plasmas should be used in order to carefully shield the growing surface from any ion bombardment, as this would create defects in the graphene and would ultimately lead towards sp3 bonding and the formation of diamond-like carbon (DLC). Thus, low temperatures and large ion bombardment leads to DLC, high temperatures and little bombardment leads to CVD diamond, while higher temperatures and catalyst leads to sp^2 bonding and graphitic carbon.

A third factor in the catalytic CVD of graphene is that the catalysis should be flat and continuous over the desired surface, and that it does not ball up as would occur in a CNT catalyst. To achieve this, the metal catalyst should be deposited on a metal such as TiN, whose similar large surface energy gives no driving force towards the de-wetting process. Kondo et al. [62] found that 15 nm was the minimum thickness needed to stop the de-wetting (Fig. 17). For higher level horizontal interconnects, it does not matter that the catalyst occupies some of the interconnect space, but it is necessary that the graphene does connect.

Ideally, it is desired to grow multi-layer graphene directly onto a dielectric substrate at low enough temperatures [63,64]. To date, no dielectric has shown enough catalytic activity to be suitable for

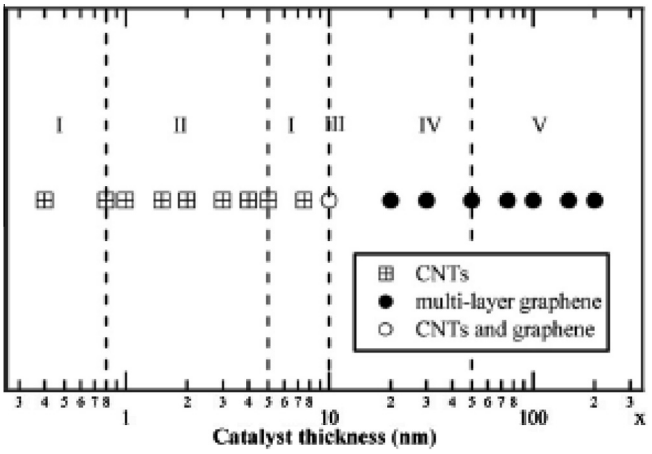

Fig. 17. Catalyst thickness growing either CNTs or graphene; showing how Co catalyst balls up if the layer below 20 nm thick on TiN, as found by Kondo.

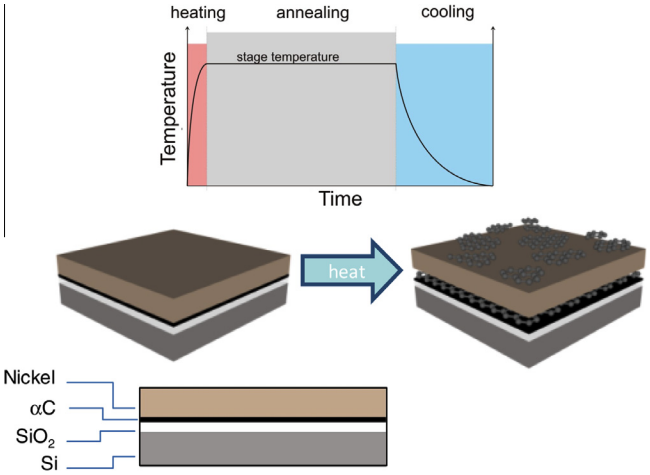

Fig. 18. Schematic of one variant of the solid state transformation of amorphous C into graphene by a Ni catalyst.

this type of growth a less than 1000 °C [63]. Plasma assisted growth is of course possible at low enough temperatures [64], but to date the grain size is rather small (5 nm) and the resulting material is 'nano-graphene'. A suitable deposition regime has still to be found.

A final possible production method of graphene is the catalytic solid state transformation [65–67], Fig. 18. This uses a metal catalyst like Ni to transform carbon into graphene, by dissolving a carbon thin film source on one side, let it diffuse across the catalyst layer, and precipitate out on the other side as graphene. This is analogous to the metal-induced crystallisation of amorphous Si into crystalline Si by silicide formers. There is some conflict in the literature about the necessary temperature. Tour et al. [65] indicate that quite high temperatures are needed. On the other hand Kwak et al. [66] claim that low temperatures (200 °C) are possible using grain boundary diffusion. However, the grain size at these low temperatures is very small. Overall, this process deserves further study as a possible production method for graphitic interconnects.

Acknowledgements

The authors are grateful to other members of the Viacarbon group, J. Dijon, H. Okuno, M. Fayolle, B. Capraro for their work, B. C. Bayer, M. Fouquet, F. Yan of Cambridge, and to the EC funding of Viacarbon and Technotubes projects. SH thanks R. Weatherup for work on graphene growth, and EPSRC for funding. We acknowledge R. Weatherup for Figs. 14, 16 and 18.

References

[1] <http://www.itrs.net/links/2009ITRS/2009Chapters_2009Tables/2009_Interconnect.pdf>.
[2] S. Frank, P. Poncharal, Z.L. Wang, W.A. deHeer, Science 280 (1998) 1744–1746.
[3] J.Y. Park, S. Rosenblatt, Y. Yaish, V. Sazonova, H. Ustunel, S. Braig, T.A. Arias, P.W. Bronner, P.L. McEuen, Nano Lett. 4 (2004) 517.
[4] A. Naeemi, J.D. Meindl, IEEE Electron Device Lett. 27 (2006) 338.
[5] B.Q. Wei, R. Vajtai, P.M. Ajayan, Appl. Phys. Lett. 79 (2001) 1172.
[6] F. Kreupl, A.P. Graham, G.S. Duesberg, W. Steinhoegl, M. Liebau, E. Unger, W. Honlein, Microelectron. Eng. 64 (2002) 339.
[7] F. Kreupl, A.P. Graham, M. Liebau, G.S. Duesberg, R. Seidel, E. Unger, Electron Dev. Meet. IEDM Tech. Dig. (2004) p683.
[8] A.P. Graham, G.S. Duesberg, R. Seidel, M. Liebau, E. Unger, F. Kreupl, W. Honlein, Diamond Relat. Mater. 13 (2004) 1296.
[9] M. Nihei, A. Kawabata, Y. Awano, Jpn. J. Appl. Phys. 42 (2003) L721.
[10] M. Nihei, M. Horibe, A. Kawabata, Y. Awano, Jpn. J. Appl. Phys. 43 (2004) 1856.
[11] D. Yokoyama, T. Iwasaki, K. Ishimaru, S. Sato, T. Hyakushima, M. Nihei, Y. Awano, H. Kawarada, Appl. Phys. Lett. 91 (2007) 263101.
[12] D. Yokoyama, T. Iwasaki, K. Ishimaru, S. Sato, T. Hyakushima, M. Nihei, Y. Awano, H. Kawarada, Jpn. J. Appl. Phys. 47 (2008) 1985.
[13] Y. Yamazaki, N. Saluma, M. Katagiri, M. Suzuki, T. Sakai, S. Sato, M. Nihei, Y. Awano, Appl. Phys. Express 3 (2010) 55002.
[14] Y. Awano, S. Sato, M. Nihei, T. Sakai, Y. Ohno, T. Mizutani, Proc. IEEE 98 (2010) 2015.
[15] G.D. Nessim, M. Seita, K.P. O'Brien, A.J. Hart, R.K. Bonaparte, R.R. Mitchell, C.V. Thompson, Nano Lett. 9 (2009) 3398.
[16] J. Robertson, G. Zhong, S. Hofmann, B.C. Bayer, C.S. Esconjauregui, H. Telg, C. Thomsen, Diamond Relat. Mater. 18 (2008) 957.
[17] J. Dijon, A. Fournier, P.D. Szkutnik, H. Okuno, C. Jayet, M. Fayolle, Diamond Relat. Mater. 19 (2010) 382. J Dijon, presented at APS (Dallas, 2011).
[18] J. Dijon, H. Okuno, E. Quesnell, M. Fayolle, T. Vo, J. Pontcharra, D. Acquiviva, A.M. Ionescu, B. Capraro, C.S. Esconjauregui, J. Robertson, Tech. Digest. IEDM (2010). p32.6.
[19] M. Fayolle, J.F. Lugand, R. Kachtouchi, H. Okuno, J. Dijon, P. Gautier, T. Billon, Proc IITC/MAM, 2011.
[20] M. Fayolle et al., Microelectron. Eng. 88 (2011) 836.
[21] J. Robertson, G. Zhong, C.S. Esconjauregui, B.C. Bayer, C. Zhang, M. Fouquet, S. Hofmann, Jpn. J. Appl. Phys. 51 (2012) 01AH01.
[22] K. Hata, D.N. Futuba, K. Mizuno, T. Namai, M. Yumura, S. Iijima, Science 306 (2004) 1362.
[23] D.N. Futaba, K. Hata, T. Yamada, T. Hiraoka, Y. Hayamizu, Y. Kakudate, O. Tanaike, H. Hatori, M. Yumura, S. Iiijima, Nat. Mater. 5 (2006) 987.
[24] T. Yamada, T. Namai, K. Hata, D.N. Futaba, K. Mizuno, J. Fan, M. Yudasaka, M. Yumura, S. Iijima, Nat. Nanotechnol. 1 (2007) 131.
[25] Y. Miyauchi, S. Chiashi, Y. Murakami, Y. Hayashida, S. Maruyama, Chem. Phys. Lett. 387 (2004) 198.
[26] S. Noda, K. Hasegawa, H. Sugime, K. Kakehi, Z.Y. Zhang, S. Maruyama, Y. Yamaguchi, Jpn. J. Appl. Phys. 46 (2007) L399.
[27] G. Zhong, T. Iwasaki, K. Honda, Y. Ohdomari, H. Kawarada, Jpn. J. Appl. Phys. 44 (2004) 1558.
[28] G. Zhong, T. Iwasaki, H. Kawarada, Carbon 44 (2006) 2009.
[29] G.F. Zhong, T. Iwasaki, J. Robertson, H. Kawarada, J. Phys. Chem. B 111 (2007) 1907.
[30] M. Cantoro, S. Hofmann, S. Pisana, V. Scardaci, A. Parvez, C. Ducati, A.C. Ferrari, A.M. Blackburn, K.Y. Wang, J. Robertson, Nano Lett. 6 (2006) 1107.
[31] J. Robertson, G. Zhong, S. Hofmann, B.C. Bayer, C.S. Esconjauregui, H. Telg, C. Thomsen, U. Detlaff, S. Roth, Appl. Phys. Lett. 93 (2008) 163111.
[32] C.T. Wirth, C. Zhang, G. Zhong, S. Hofmann, J. Robertson, ACS Nano 3 (2009) 3560.
[33] S. Sato, A. Kawabata, M. Nihei, Y. Awano, Chem. Phys. Lett. 382 (2003) 361; D. Kondo, S. Sato, Y. Awano, Chem. Phys. Lett. 432 (2006) 481.
[34] A.L. Giermann, C.V. Thompson, Appl. Phys. Lett. 86 (2005) 121903.
[35] C. Mattevi, C.T. Wirth, S. Hofmann, R. Blume, M. Canotro, C. Ducati, C. Cepek, A. Knop, S. Milne, C. Castellarin-Cudia, S. Dolafi, A. Goldoni, R. Schlogl, J. Robertson, J. Phys. Chem. C 112 (2008) 12207.
[36] G. Zhong, J.H. Warner, M. Fouquet, A.W. Robertson, B. Chen, J. Robertson, ACS Nano 6 (2012) 2893.
[37] S. Esconjauregui, M. Fouquet, B.C. Bayer, C. Ducati, R. Smajda, S. Hofmann, J. Robertson, ACS Nano 4 (2010) 7431.
[38] C. Zhang, R. Xie, J. Robertson, unpublished work.
[39] S. Esconjauregui, B.C. Bayer, C.T. Wirth, S. Hofmann, J. Robertson, Appl. Phys. Lett. 95 (2009) 173115.
[40] C.S. Esconjauregui, M. Fouquet, B.C. Bayer, E. Eslava, S. Khachadorian, S. Hofmann, J. Robertson, J. Appl. Phys. 109 (2011) 044303.
[41] C.S. Esconjauregui, B.C. Bayer, M. Fouquet, C.T. Wirth, F. Yan, R. Xie, C. Ducati, C. Cepek, S. Hofmann, J. Robertson, J. Appl. Phys. 109 (2011) 114312.
[42] J. Dijon, P.D. Szkutnik, A. Founrier, Carbon 48 (2010) 3953.
[43] B.C. Bayer, C. Zhang, R. Blume, F. Yan, M. Fouquet, C.T. Wirth, R.S. Weatherup, L. Lin, C. Baehtz, R.A. Oliver, A. Knop, R. Schlogl, S. Hofmann, J. Robertson, J. Appl. Phys. 109 (2011) 114314.
[44] B.C. Bayer, S. Hofmann, C. Castellarin-Cudia, R. Blume, C. Baehtz, S. Esconjauregui, C.T. Wirth, R.A. Oliver, C. Ducati, A. Knop, R. Schlogl, A. Goldoni, C. Cepek, J. Robertson, J. Phys. Chem. C 115 (2011) 4359.
[45] C. Zhang, F. Yan, B.C. Bayer, J. Robertson, J. Appl. Phys. 111 (2012) 064310.
[46] F. Yan, C. Zhang, D. Cott, G. Zhong, J. Robertson, Phys. Status Solidi B 247 (2010) 2669;
C. Zhang, D. Cott, N. Chiodarelli, P. Vereecken, J. Robertson, C.M. Whelan, Phys. Status Solidi B 245 (2008) 2308.
[47] C. Santini, D. Cott, A. Romo-Negreira, B.D. Capraro, S.R. Sanseverino, S. DeGendt, G. Groesenken, P.M. Vereecken, Nanotechnology 21 (2010) 245604.
[48] C.A. Santini, A. Volodin, C. van Hesse, G. Groeseneken, P.M. Vereekcken, Carbon 49 (2011) 4004.
[49] Y. Hayamizu, T. Yamada, K. Mizuno, R.C. Davis, D.N. Futaba, M. Yumura, K. Hata, Nat. Nanotechnol. 3 (2008) 289.
[50] A.P. Graham, G. Schindler, G.S. Duesberg, T. Lutz, W. Weber, J. Appl. Phys. 107 (2010) 114316.
[51] A. Reina, X. Jia, J. Ho, D. Nezich, H. Son, V. Bulovic, M.S. Dresselhaus, J. Kong, Nano Lett. 9 (2009) 30.
[52] X. Li, W. Cai, J. An, S. Kim, J. Nah, H. Son, D. Yang, E. Tutuc, S. Banerjee, L. Colombo, R. Ruoff, Science 324 (2009) 1312.
[53] X. Li, W. Cai, L. Colombo, R. Ruoff, Nano Lett. 9 (2009) 4268.
[54] X. Li, C.W. Magnusson, A. Venugopal, J. An, J.W. Suk, B. Han, M. Borysiak, W. Cai, A. Velamakanni, Y. Zhu, L. Fu, E.M. Vogel, E. Voekl, L. Colombo, R.S. Ruoff, Nano Lett. 10 (2010) 4328.
[55] R.S. Weatherup, B.C. Bayer, R. Blume, C. Ducati, C. Baehtz, R. Schlogl, S. Hofmann, Nano Lett. 11 (2011) 4154.

[56] M. Batzill, Surf. Sci. Rep. 67 (2012) 83.
[57] J. Robertson, J. Mater. Chem. 22 (2012) 19858.
[58] D. Kondo, S. Sato, Y. Awano, Appl. Phys. Express 1 (2008) 074003.
[59] D. Kondo, S. Sato, K. Yagi, N. Harada, M. Sato, M. Nihei, N. Yokoyama, Appl. Phys. Express 3 (2010) 025102.
[60] Y. Kim, W. Song, S.Y. Lee, C. Jeon, W. Jung, M. Kim, C.Y. Park, Appl. Phys. Lett. 98 (2011) 263106.
[61] J. Kim, M. Ishihara, Y. Koga, K. Tsugawa, M. Hasegawa, S. Iijima, Appl. Phys. Lett. 98 (2011) 091502.
[62] D. Kondo, K. Yagi, M. Sabo, M. Nihei, Y. Awano, S. Sato, Chem. Phys. Lett. 514 (2011) 294.
[63] M. Rummeli, Chem. Mater. 19 (2007) 4106.
[64] H. Medina, Y.C. Lin, C. Jin, C.C. Lu, C.H. Yeh, K.P. Huang, K. Suenaga, J. Robertson, P.W. Chiu, Adv. Funct. Mater. 22 (2012) 2123.
[65] J.M. Tour, ACS Nano 5 (2011) 8187.
[66] J. Kwak, Nat. Commun. 3 (2012) 645.
[67] J.M. Tour, J. Phys. Chem. Lett. 2 (2011) 2425.